

# DEVELOPMENT OF HIGH THERMAL EFFICIENCY IMPINGING JET NOZZLE FOR HOT AIR DRYING OF GRAVURE PRINTING

SATORU INOUE, KATSUhide EGUCHI AND TSUNEHiko IMAMOTO

*Engineering Research Laboratory, Dai Nippon Printing Co., Ltd.  
Tokyo 115*

**Key Words:** Heat Transfer, Drying, Nozzle, Turbulence Promotion, Gravure Printing, Energy

A high thermal-efficiency impinging jet nozzle was developed by a study of nozzle structure in order to devise a photogravure press and coater-dryer of energy-saving type.

Aiming at an expansion of the high heat transfer range and turbulence promotion compared to the existing slit nozzle, a high-performance impinging jet nozzle with a heat transfer coefficient 1.5 times that of a slit nozzle was acquired through analysis and examination of the phenomenon of impinging jet heat transfer by means of trial production of about 40 kinds of nozzle, measurement of heat transfer coefficient, visualization of flow and heat transfer pattern, and measurement of jet velocity and turbulence distribution.

## Introduction

Dryers of hot-air type are dominant in use for the photogravure press. Their thermal efficiency, however, is quite low and most of the input energy is wasted as exhaust or radiation.

An investigation of traditional dryers proved the following points: 1) Most dryer nozzles consist of simple slit nozzles, and nozzle pitch lacks uniformity among different machines, which cannot be fully adaptive to the complicated mechanism of ink drying and heat transfer. 2) Drying capacity  $R$  is nearly proportional to input energy where thermal efficiency is not taken into account.

A nozzle with large heat transfer coefficient was developed, based on analysis of the heat transfer phenomenon of an impinging jet from the nozzle. The present paper describes how this nozzle was developed.

## 1. Experimental Method

Drying rate is proportional to the heat transfer coefficient  $\alpha$  in the constant drying rate period, and it is an important factor even in the falling drying rate period. Moreover,  $\alpha$  in an impinging jet can be given by Eq. (1) according to Gardon,<sup>1,2)</sup> Saad<sup>9)</sup> and others:<sup>6,8)</sup>

$$\alpha = cG^{0.67-0.78} \quad (1)$$

Where  $c$  is nozzle coefficient. Its value depends on nozzle form, distance between nozzle and target plate

and nozzle pitch, etc.

The purpose of this development was to increase  $\alpha$  as well as to improve drying capacity without increasing fan power or thermal energy.

Nozzle performance was evaluated synthetically by means of a mutual comparison between  $\alpha$  and  $L$ , which were measured in the case where average mass velocity of photogravure press dryer  $G_s = 2700 \text{ kg/m}^2 \cdot \text{h}$  was given. The experimental apparatus is shown in Fig. 1. It consisted mainly of three nozzles (150 mm width) and four exhaust ports. It was constructed so that various measurements and evaluations could be carried out under the nozzle mounted in the center. It was to reproduce one nozzle among an infinite number of nozzles, covering the influence of nozzles installed on both sides, that three nozzles were installed. Exchange of nozzles as well as the alteration of nozzle opening width and distance between nozzle and target plate could be easily made in this apparatus.

### 1.1 Measurement of heat transfer coefficient and required fan power

Measurement of the heat transfer coefficient was conducted on a stainless steel foil (fixed on acrylic plate with adhesive tape) of  $30 \mu\text{m}$  thickness, heated directly by AC. The foil was placed under the center nozzle of the experimental apparatus mentioned above. The surface temperature of stainless steel foil  $T_s$  was measured, when a jet at normal temperature impinged on it from the nozzle, by copper-constantan thermocouples of  $80 \mu\text{m}$  diameter soldered on the rear side of the foil.  $\alpha$  is determined from Eq. (2):

Received February 12, 1988. Correspondence concerning this article should be addressed to S. Inoue.

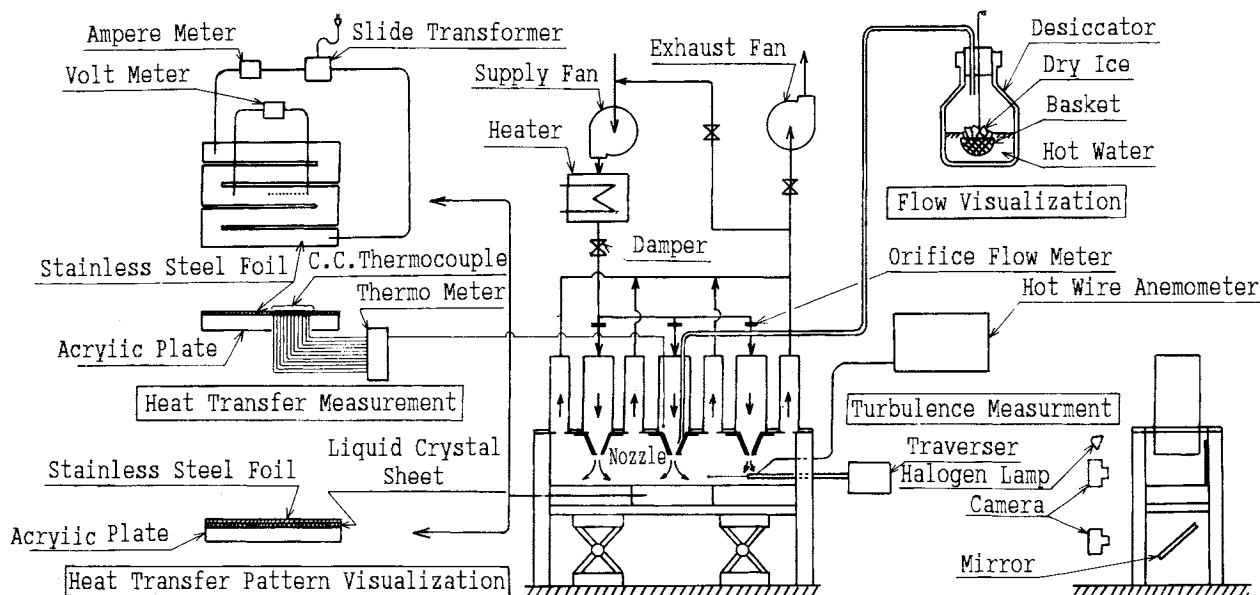


Fig. 1. Experimental Apparatus

$$\alpha = IV/A(T_s - T_a) \quad (2)$$

Fan power  $L$  is given by Eq. (3):

$$L = U_e A_f \phi(p_n + p_a)/\eta_f \eta_t \quad (3)$$

## 1.2 Visualization of flow pattern

The following three methods were adopted at the same time:

- white smoke method with dry ice (main method)
- tufting method for local visualization
- wall tracing method for target plate surface

1) White smoke method with dry ice As shown in Fig. 1, this method allows observation of the trace of white smoke that spouts from the nozzle with the jet. Crushed dry ice was immersed instantly in hot water, and the white smoke produced was sent through a rubber hose to the nozzle, mixed with compressed air by a fan and jetted from the nozzle.

2) Tufting method Flow direction and turbulence intensity were measured under the nozzle by observing the direction and sway of a tuft consisting of nylon fiber stuck on the end of a piano wire.

3) Wall tracing method An acrylic plate coated with trace liquid which was a mixture of titanium oxide, liquid paraffin and oleic acid was placed under the nozzle and the surface pattern of the trace liquid was observed after a jet impingement during a certain period (1–10 min).

## 1.3 Visualization of heat transfer pattern

A jet at normal temperature was applied to stainless steel foil heated directly by current, to which a liquid crystal sheet was stuck. Temperature distribution on the foil was observed by alteration in the color of the liquid crystal sheet (blue-green-amber-brown in the range of 313 K–318 K). Because the

nozzle was installed just above the liquid crystal sheet, visualization from the upper side was impossible. Color alteration of the liquid crystal sheet was therefore observed from the front of the experimental apparatus by means of a mirror installed below.

## 1.4 Measurement of turbulence intensity

A probe ( $5 \mu\text{m}\phi$ ) consisting of a wire anemometer was installed between nozzle and target plate. It was traversed perpendicularly and vertically by a DC motor. Flow velocity of each part  $U$  and root mean square of the axial fluctuating velocity component  $U'$  were registered on an oscillograph.

## 2. Development of High Thermal Efficiency Impinging Jet Nozzle

Measurement and evaluation of  $\alpha$ -distribution and  $U'$ , etc., were made for a row of traditional slit nozzles. Values have been reported by Gardon,<sup>1,2)</sup> Saad<sup>9)</sup> and others and test results outside the scope of their document and report proved the following: 1) As shown in Fig. 2,  $\alpha$  is locally large just under the nozzle but falls extremely at other locations. 2) Most flow in the range of  $\zeta/B < 2$  and  $U'/U_e$  value on the target plate is considerably low.

Based on these results, the development plan for an efficient impinging jet nozzle was framed as follows: 1) An expansion of the range having high heat transfer coefficient by improvement of  $\alpha$  in other locations, as against the traditional slit nozzle for which  $\alpha$  is large only just under the nozzle. 2) Promotion of turbulence on the target plate and destruction of boundary layer.

Trial making of various kinds of nozzle, their evaluation and investigation were conducted repeatedly according to these plans. The following are the results of overall evaluation based on the test

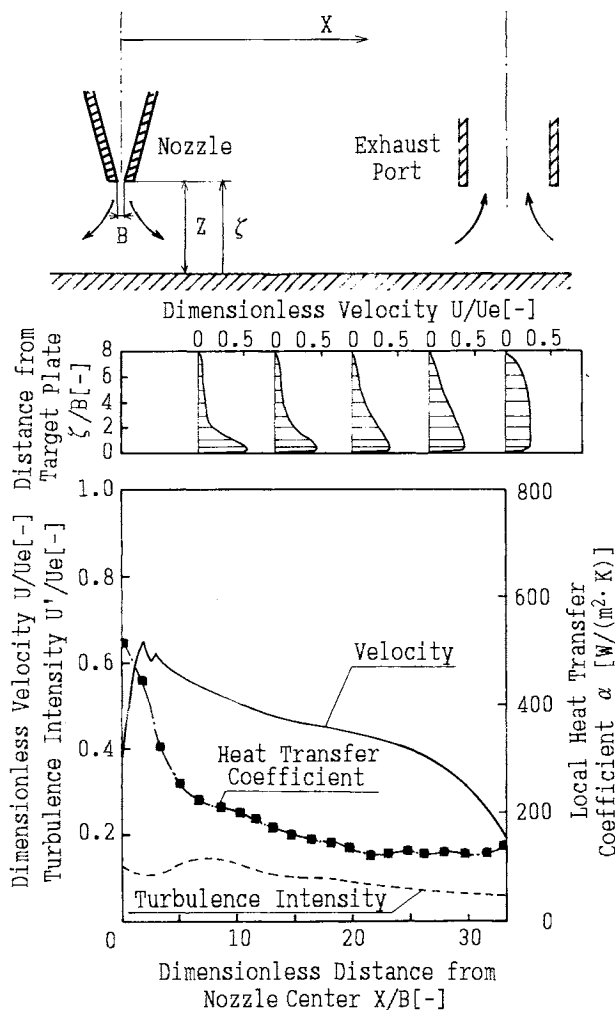


Fig. 2. Flow and local heat transfer distribution curves of slit nozzle

results for each nozzle and their comparison.

The effects of turbulence on heat transfer have been investigated by several workers. Kestin<sup>4,5)</sup> showed that it can affect heat transfer in two ways: 1) In the absence of pressure gradients—as, for example, over a flat plate parallel to the flow—increased turbulence in the free stream tends to promote the transition from a laminar to a turbulent boundary layer. The distribution of local heat transfer coefficients is affected only to the extent of the forward shift of the point of transition. 2) In the presence of pressure gradients, such as may be found on a flat plate in an accelerating stream, increasing free stream turbulence also has a direct effect on local heat transfer coefficients, increasing them without causing an irreversible change in the character of the boundary layer.

### 2.1 Turbulence-promotion nozzle

The following test was conducted with the aim of improving  $\alpha$  by promoting turbulence intensity.<sup>3)</sup> The following three means for turbulence promotion were adopted: 1) punched plate between nozzle and target plate; 2) net between nozzle and target plate; and 3)

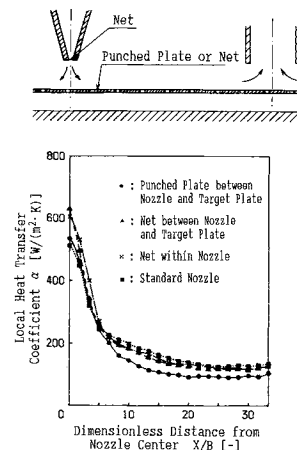


Fig. 3. Local heat transfer distribution curves of turbulence promotion nozzle

net within nozzle.

As shown in Fig. 3,  $\alpha$  increased in each case, near the stagnation point but fell in other locations, and  $\bar{\alpha}$  proved to be the same as or less than that of the slit nozzles.

To analyze the cause of degradation of  $\alpha$  in the punched plate, a flow visualization under the nozzle was conducted using the tufting method as well as the dry-ice method. Intensification of turbulence was confirmed by sway of tuft, but at the same time the flow velocity on the target plate was reduced because flow on the upper side of the punched plate was too strong and a considerable amount of air was exhausted toward the upper part of the punched plate. In other words, in spite of local augmentation of  $\alpha$  near the stagnation point by turbulence promotion, it was thought that  $\alpha$  in other locations was reduced, and that  $\bar{\alpha}$  fell in consequence because the impinging jet velocity against the target plate was reduced due to the action of the punched plate as a barrier.

### 2.2 Enforcement parallel-flow nozzle

The following test was conducted with the aim of improving  $\alpha$  in locations other than the point just under the nozzle by increasing the parallel flow velocity on the target plate, the space on the target plate being reduced between the nozzle and exhaust port. As shown in Fig. 4, a squeeze plate was placed between nozzle and exhaust port, and the distance between squeeze plate and target plate was fixed at  $Z'/B = 1/2$  and 1. With  $Z'/B = 1/2$ ,  $\alpha$  rose all over the target plate and  $\bar{\alpha}$  also improved by a remarkable 49%.

### 2.3 Baffle nozzle

The following experiment was performed for the purpose of expanding the high heat-transfer range. A baffle plate was installed above the target plate, enabling the flow to impinge once on the target plate and to impinge on it again in vertical fashion.

As a result,  $\alpha$  increased just behind the baffle plate

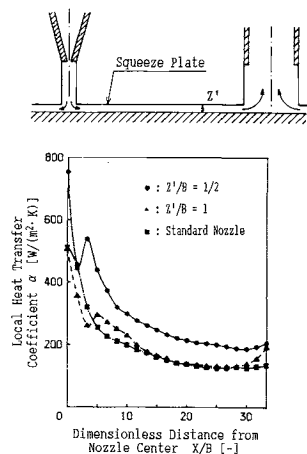


Fig. 4. Local heat transfer distribution curves of enforcement parallel flow nozzle

in the case of  $Z'/B = 2/3$  and  $\bar{\alpha}$  became 9% higher than that for the slit nozzle, as shown in Fig. 5.

Figure 6 shows photos of visualized flow of the baffle nozzle in comparison with the slit nozzle. Regarding the slit nozzle shown at the upper left of Fig. 6, the air (white smoke) jetted downward from the nozzle, impinged on the target plate, flowed along the target plate and was discharged from the exhaust port. Concerning the baffle nozzle shown at the lower left, as against the above, the flow direction was changed by the baffle at the center while the air was flowing along the plate, causing the air to jet onto the target plate. Supposedly, promotion of boundary layer destruction caused  $\alpha$  to increase just behind the baffle.

Moreover, the baffle was punched or twisted in order to promote turbulence, but compared with a plain baffle the increase in ratio of  $\alpha$  just behind the baffle was low. And  $\bar{\alpha}$  was even reduced a little.

#### 2.4 Multiple-slit nozzle

The following experiment was conducted with the aim of expanding the range of higher heat transfer by means of multiplication of nozzles.

Alteration of  $\alpha$  was measured for combinations of two to five nozzles, the opening width being fixed at 1 mm. As shown in Fig. 7, the larger the number of nozzles, the larger was the number of peaks at the same value of  $G$ . The value of each peak, however, tended to be lower, and the fewer the nozzles, the higher  $\bar{\alpha}$  became. This is probably because more nozzles meant a larger nozzle open-area ratio  $A$ ; i.e. flow velocity was reduced.

#### 2.5 Multiple staggered-slit nozzle

The following experiment was conducted with the aim of producing a three-dimensional impingement of air in the lower heat transfer range among the jet ports and to increase  $\alpha$ , in addition to the increase of  $\alpha$  by expansion of the high heat-transfer range in the case of the multiple-slit nozzle mentioned above.

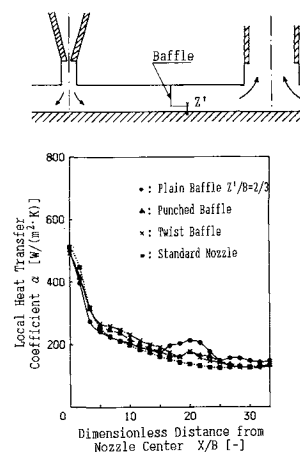


Fig. 5. Local heat transfer distribution curves of baffle nozzle

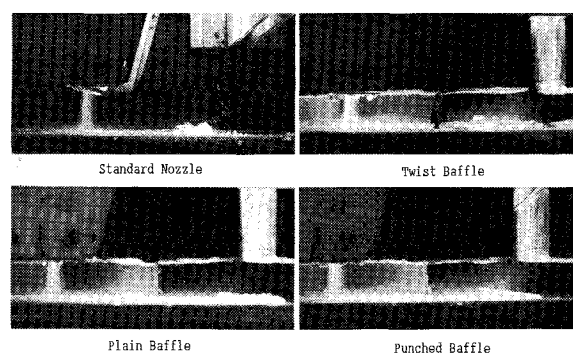


Fig. 6. Flow visualization of baffle nozzle

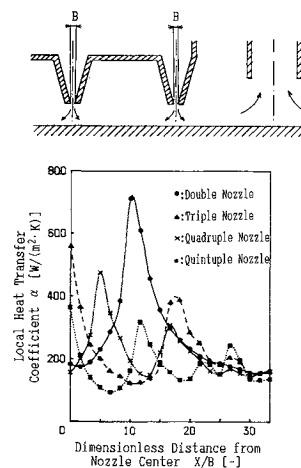


Fig. 7. Local heat transfer distribution curves of multiple slit nozzle

As shown in Fig. 8,  $\alpha$  increased in overall range in the case of the rectangular-hole nozzle in comparison with the multiple-slit nozzle. As for the circular-hole nozzle,  $\alpha$  increased considerably between the central jet port and the side ports. In each case,  $\bar{\alpha}$  became still higher than that of the multiple-slit nozzle by about 30%.

Secondly, visualization by the wall-tracing method

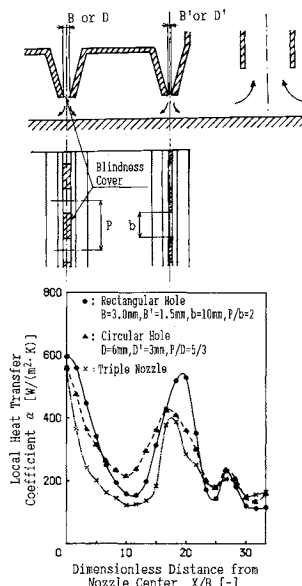


Fig. 8. Local heat transfer distribution curves of multiple staggered slit nozzle

of two-dimensional flow on the target plate is shown in Fig. 9 in comparison with the standard slit nozzle. The black part indicates that trace liquid was spread by the jet. The wind from the central impinging port and that from both sides were crossing in a wedge pattern and a remarkable intensification of turbulence at this point was indicated by the tuft.

Further, photos of the visualized heat transfer pattern by the liquid crystal method are shown in Fig. 10.  $\alpha$  is higher in the chocolate part and lower in the blue part. For the slit nozzle,  $\alpha$  is high only just under the nozzle center and is low elsewhere, whereas the present nozzle proves to have a range with high  $\alpha$  that is extended and staggered all over the surface.

## 2.6 Punched-plate nozzle

The following experiment was conducted on a punched-plate nozzle with the aim of making its manufacture and cleaning easier and its hole arrangement more flexible.

$\alpha$  was measured with a 0.015 fixed open-area ratio of nozzle and the parameters of orifice diameter  $D$  and distance between nozzle and target plate  $Z/B$ . The orifice diameters were chosen as 3 mm and 5 mm, taking convenience of manufacturing and cleaning into account, though the smaller the orifice diameter, the less is the drying unevenness caused by jet velocity distribution in width-wise direction of the nozzle.  $\alpha$  was measured where  $Z$  was varied among 4 mm, 8 mm, 16 mm and 24 mm for each diameter.

As a result, the smaller the value of  $Z$ , the higher  $\alpha$  tended to be for both orifice diameters,  $D=3\text{ mm}$  and  $D=5\text{ mm}$ . A slight degradation of  $\alpha$  was observed, however, where  $D=5\text{ mm}$  and  $Z=4\text{ mm}$ . Concerning the influence of  $D$ ,  $\alpha$  was, at the same  $Z/D$ , a little higher for  $D=3\text{ mm}$  than for  $D=5\text{ mm}$ . On the

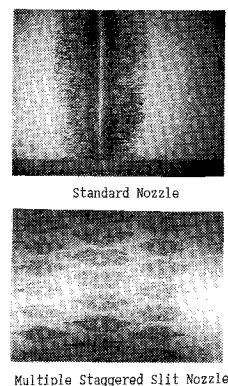


Fig. 9. Flow visualization of multiple staggered slit nozzle

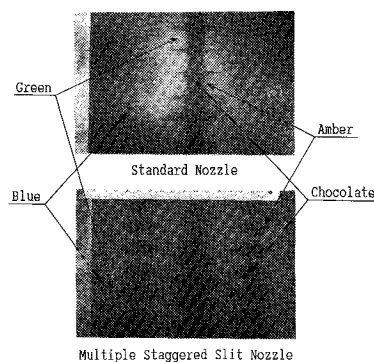


Fig. 10. Heat transfer visualization of multiple staggered slit nozzle

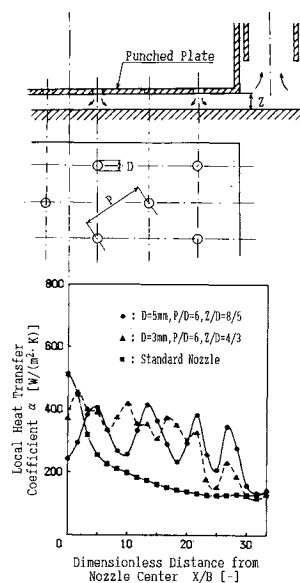


Fig. 11. Local heat transfer distribution curves of punched plate nozzle

contrary,  $\alpha$  had a tendency, at the same  $Z$ , to be higher for  $D=5\text{ mm}$  than for  $D=3\text{ mm}$ .

Figure 11 shows the measurement results of local  $\alpha$  for  $D=5\text{ mm} \cdot Z=8\text{ mm}$  and  $D=3\text{ mm} \cdot Z=4\text{ mm}$ , which proved to be the best value combinations by the measurement mentioned above. In each case,  $\alpha$  reaches a higher value owing to a remarkable expan-

sion of the high heat-transfer range. For  $D=3$  mm, the peaks are more numerous as are the holes, and the difference between top and bottom is smaller. As for the distribution in width-wise direction of the nozzle in the case of  $D=5$  mm, a countermeasure should be worked out because these nozzles might cause drying unevenness in width-wise direction when used in a dryer.

## Conclusion

To evaluate the performance of each nozzle concerning energy based on the experiments described above,  $\alpha$  and  $L$  for each nozzle are shown in Fig. 12. The equal-energy curve in the figure is drawn by linking the points where total energy is equivalent in amount to that of the slit nozzle based on a balance between  $\alpha$  and  $L$ , according to the following method.

From the experiments conducted in the present study,  $\alpha$  can be defined as

$$\alpha = cG^{0.78} \quad (4)$$

where  $G=2000\text{--}4000\text{ kg/m}^2\cdot\text{h}$  in the case of the slit nozzle and the punched-plate nozzle. This agrees with the experimental results of Saad and others. That is, hot air mass velocity  $G'$  required to obtain  $\alpha_s=192\text{ W/m}^2\cdot\text{K}$  (at standard slit nozzle,  $G_s=2700\text{ kg/m}^2\cdot\text{h}$ ) by using another kind of nozzle is given by Eq. (5):

$$G' = G_s(\alpha_s/\alpha')^{1/0.78} \quad (5)$$

Input heat energy for dryer  $Q$  is given by Eq. (6):

$$Q = G' C_p (T_a - T_o)(1 - e_e e_r) \quad (6)$$

The overall energy  $E$  is then given by Eq. (7):

$$E = Q + k \cdot L \quad (7)$$

The equal-energy curve was drawn according to Eq. (8), based on Eqs. (5)–(7).

$$\alpha' = \left\{ \frac{\alpha_s^{1/0.78} G_s C_p (T_a - T_o)(1 - e_e e_r)}{E - kL} \right\}^{0.78} \quad (8)$$

The punched-plate nozzle, multiple staggered-slit nozzle, double nozzle and enforcement parallel-flow nozzle ( $Z'/B=1/2$ ) are regarded as nozzles having higher  $\alpha$ . With regard to the double nozzle and the enforcement parallel flow nozzle, however, the energy efficiency is not particularly improved by increase of fan power. The punched plate has, after all, the best energy efficiency because its fan power increases little and  $\alpha$  rises by more than 50%. The multiple staggered-slit nozzle, multiple-slit nozzle, etc. are second to the punched-plate nozzle in energy efficiency.

An analysis of the ink drying phenomenon<sup>7)</sup> was carried out at the same time as the experiments for development of a high-performance impinging jet nozzle.

A dryer having excellent drying efficiency—about

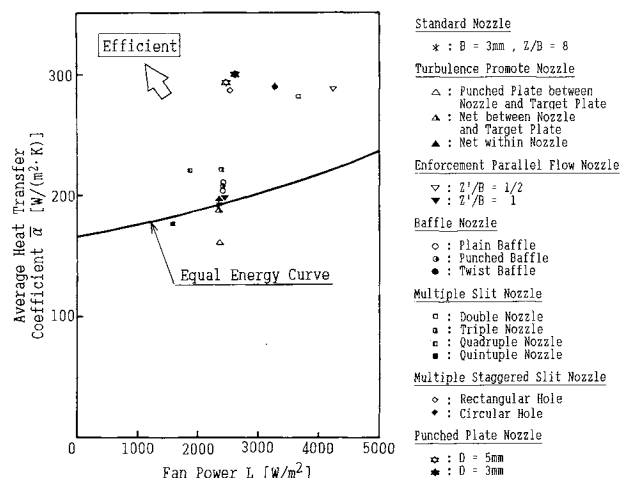


Fig. 12. Efficiency of each test nozzle

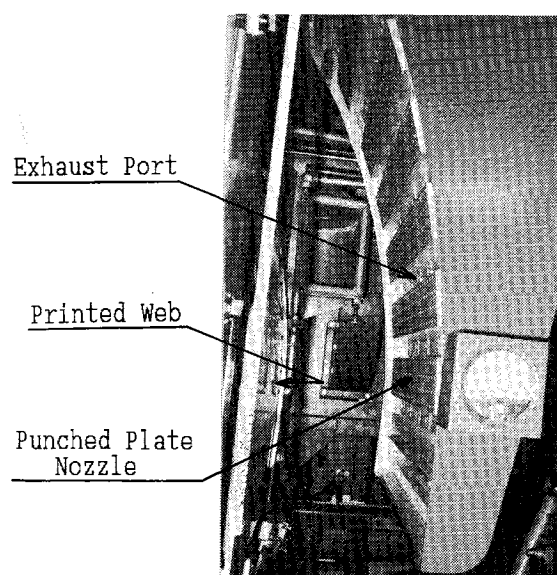


Fig. 13. New dryer with punched plate nozzle

twice that of existing dryers—has finally been developed. Figure 13 shows the appearance of the drying hood for such a dryer. For the moment, it is equipped with seven photogravure presses and one coater, its drying performance and energy-saving effect being greatly enhanced.

## Acknowledgments

The authors wish to thank Ryozi Toei, Professor Emeritus, and Prof. Morio Okazaki, of the Chemical Engineering Department of Kyoto University, and Prof. Masaru Hirata of the Mechanical Engineering Department of Tokyo University, for their help in the present work.

## Nomenclature

$A$	= measurement surface area of stainless steel foil	[m <sup>2</sup> ]
$A_f$	= open area ratio $B/X$	—
$B$	= nozzle slit width	[mm]
$C_p$	= specific heat capacity of air at constant pressure	[kJ/(kg·K)]

$c$	= nozzle coefficient	[—]
$D$	= orifice diameter	[mm]
$E$	= total energy	[kJ/(m <sup>2</sup> ·h)]
$e_e$	= output heat energy/input heat energy at dryer	0.7 [—]
$e_r$	= recycling ratio of exhaust gas	0.3 [—]
$G$	= mass velocity	[kg/(m <sup>2</sup> ·h)]
$G'$	= required mass velocity to obtain $\alpha_s = 192 \text{ W}/(\text{m}^2 \cdot \text{K})$ by using each test nozzle	[kg/(m <sup>2</sup> ·h)]
$G_s$	= mass velocity of standard condition	[kg/(m <sup>2</sup> ·h)]
$I$	= current intensity	[A]
$k$	= unit conversion efficiency	3.6 [kJ/(W·h)]
$L$	= required fan power	[W/m <sup>2</sup> ]
$p_n$	= pressure drop across nozzle	[pa]
$p_d$	= pressure drop across duct	980 [pa]
$Q$	= input heat energy to dryer	[kJ/m <sup>2</sup> ·h]
$Re$	= Reynolds number $Bu\rho/\mu$ , $Du\rho/\mu$	[—]
$T_a$	= nozzle exit temperature	[K]
$T_o$	= input air temperature for dryer	293 [K]
$T_s$	= surface temperature of stainless steel foil	[K]
$U$	= velocity	[m/s]
$U_e$	= nozzle exit velocity	[m/s]
$U'$	= root mean square of axial fluctuating velocity	[m/s]
$U'/U_e$	= turbulence intensity	[—]
$V$	= potential drop across measurement surface area	[V]
$X$	= nozzle pitch	[mm]
$Z$	= distance between nozzle and target plate	[mm]
$Z'$	= distance between punched plate, net, squeeze plate, baffle and target plate	[mm]

$\alpha$	= local heat transfer coefficient	[W/(K·m <sup>2</sup> )]
$\alpha'$	= average heat transfer coefficient of each test nozzle at $G = 2700 \text{ kg}/(\text{m}^2 \cdot \text{h})$	[W/(K·m <sup>2</sup> )]
$\alpha_s$	= average heat transfer coefficient of slit nozzle at $G = 2700 \text{ kg}/(\text{m}^2 \cdot \text{h})$	[W/(K·m <sup>2</sup> )]
$\bar{\alpha}$	= average heat transfer coefficient	[W/(K·m <sup>2</sup> )]
$\eta_f$	= fan pressure efficiency (turbofan)	0.65 [—]
$\eta_i$	= fan belt transfer efficiency (V belt)	0.95 [—]
$\phi$	= fan safety ratio	1.15 [—]

#### Literature Cited

- 1) Gardon, R. and J. C. Akfirat: *International Journal of Heat and Mass Transfer*, **8**, 1261 (1965).
- 2) Gardon, R. and J. C. Akfirat: *Journal of Heat Transfer, A.S.M.E*, Series C, 101 (1966).
- 3) Kahn, M. M. Ali., N. Kasagi, M. Hirata and N. Nishiwaki: *Heat Transfer 1982*, **3**, 363 (1982).
- 4) Kestin, J., P. F. Maeder and H. E. Wang: *International Journal of Heat and Mass Transfer*, **3**, 133 (1961).
- 5) Kestin, J., P. F. Maeder and H. H. Sogin: *Z. Angew. Math. Phys.*, **12**, 115 (1961).
- 6) Obot, N. T., A. S. Mujumdar and W. J. M. Douglas: *Drying* **80**, **1**, 388 (1980).
- 7) Okazaki, M., K. Shioda, K. Masuda and R. Toei: *Journal of Chemical Engineering of Japan*, **7**, 99 (1974).
- 8) Pinter, R. and R. Greimel: *Proceedings of The Third International Drying Symposium*, **1**, 575 (1982).
- 9) Saad, N. R., A. S. Mujumdar and W. J. M. Douglas: *Drying* **80**, **1**, 422 (1980).